

SUPPLEMENTAL MATERIAL

Meier, et al. CD301b/MGL2⁺ mononuclear phagocytes orchestrate autoimmune cardiac valve inflammation and fibrosis.

SUPPLEMENTAL METHODS

Intracellular cytokine staining (ICS)

For analysis of TNF and IL-6 production *in vivo*, a bolus of 250 µg brefeldin A (eBioscience, 00-4506-51) in 200 µL saline was injected into the peritoneal cavity of each animal three hours prior to euthanasia. Lymphoid tissues and hearts were excised and prepared as described above.

For ICS experiments, all sample buffers used prior to sample fixation contained 3 µg/mL brefeldin A. After staining surface antigens, samples were fixed and permeabilized as described above. Anti-TNF (clone MP6-XT22, BioLegend), and anti-IL-6 (clone MP5-20F3, BioLegend) antibodies were added at 1 µg/mL for 30 minutes at room temperature, protected from light. Each sample was subsequently washed three times using PBS containing 2% BSA, filtered through a 70 µm cell strainer, and used for flow cytometry analyses as described above.

Human heart valve histology

De-identified human cardiac valve samples were acquired by CardioStart International during charitable missions in countries with high incidences of rheumatic cardiac disease presentation. Samples were taken from patient's valves being explanted during surgical correction (all harvesting followed University of Minnesota's patient consent procedures directed by UMN IRB no: 1307M39481). Histological analyses of these samples were deemed exempt from University of Minnesota Institutional Review Board oversight due to the de-identified nature of the samples. Following surgical resection, samples were placed in 10% neutral buffered formalin for short-term storage and for transportation to the laboratory. Each sample was subsequently placed in 70% ethanol until paraffin embedding and sectioning. Formalin-fixed, paraffin-embedded (FFPE) samples were sectioned at 7 µm, deparaffinized in xylene, and rehydrated using a decreasing ethanol/water gradient. Masson's trichrome staining was performed as described above. For IF, antigen retrieval was conducted according to the manufacturer's protocol (R&D

Systems, #CTS015, Antigen Retrieval Reagent-Universal). Briefly, samples were incubated in neutral antigen retrieval buffer for 10 minutes at 95°C. After cooling, Fc receptors were blocked for 30 minutes at room temperature (Innovex, #NB309). Samples were then washed using PBS containing 1% BSA and 2% FBS. Blocking of non-specific interactions was accomplished using 5% normal goat serum (Jackson Immunoresearch) and 2% BSA in PBS for 30 minutes at room temperature. Mouse-anti-human CD163 (ThermoFisher #MA5-11458, clone 10D6) and rabbit-anti-human CD301/CLEC10A (Abcam, ab197346, anti-CLEC10A) were applied overnight at 4°C in a humidified staining box at a 1:25 dilution of the stock antibody solution into PBS containing 1% BSA and 2% FBS. Nuclei were counterstained using mounting medium containing DAPI (Vector Laboratories). Sections were imaged using epifluorescence microscopy (Leica DM6000B).

Tissue clearing and mitral valve whole-mount imaging

Following euthanasia and prior to excision, hearts from *Cx3cr1^{+gfp}* mice were perfused with 4% paraformaldehyde (PFA) in PBS, excised, and placed in fresh 4% PFA in PBS for 10 minutes on ice with continuous mixing. Samples were subsequently post-fixed overnight after replacing the 4% PFA in PBS. Whole MVs were isolated and the isolated MVs were washed extensively in PBS prior to clearing according to methods described previously¹ with minor modifications. Briefly, samples were incubated in 4% acrylamide solution (Sigma) with the thermal initiator VA-044 at 0.25% (Wako Chemical, NC0632395) for 4 hours at 4°C. Fresh, degassed acrylamide solution was replaced and polymerized for 3 hours at 37°C. Any remaining acrylamide solution was removed with PBS washes. The polymerized samples were then incubated for 6 hours in 200 mM sodium dodecyl sulfate (SDS) solution buffered with 20 mM boric acid (pH 8.4). Next, the samples were incubated for 24 hours at 37°C in a solution containing 5% N,N,N',N' tetrakis ethylenediamine (Sigma), 10% urea, 10 mM SDS, 2% Triton X-100, and 20 mM boric acid buffer (pH 8.4). The cleared tissue was extensively washed using PBS containing 0.5% Triton

X-100. The processed tissue refractory index was matched using 88% Histodenz solution (Sigma, D2158) for embedding. A Leica DM6000B epifluorescence microscope was employed to image the atrial surface of the valves. Due to the uneven topology of the whole-mount, a maximum intensity z-projection from 10 focal planes was constructed and pseudo-colored to generate the image in Figure 2B.

Bone marrow chimeras

Two sets of experiments involving bone marrow (BM) chimeras were employed. In the first, *Tnfr1*-deficient and control animals on the *Rag1*^{-/-} background were reconstituted with K/B.g7 bone marrow. In the second, mice bearing the congenic *Ptprc*^{b/b} (CD45.2^{+/+}) allele on the C57Bl/6 *Rag1*^{-/-} background were reconstituted with bone marrow from mice bearing the congenic *Ptprc*^{a/a} (CD45.1^{+/+}) allele on the K/B.g7 background. In both cases, 6-week-old bone marrow recipient mice were sub-lethally irradiated (300 rads). After four hours and under isoflurane anesthesia, each irradiated animal was reconstituted with 5x10⁶ bone marrow cells via retro-orbital injection. Mice were maintained on oral trimethoprim-sulfamethoxazole (TMP-SMX) during the engraftment period. Hearts were collected for histology following 10 weeks of reconstitution. Arthritis progression was assessed weekly throughout the experimental duration. Serum samples were collected at the experimental endpoint following euthanasia to assess anti-GPI IgG titers.

Image Analysis

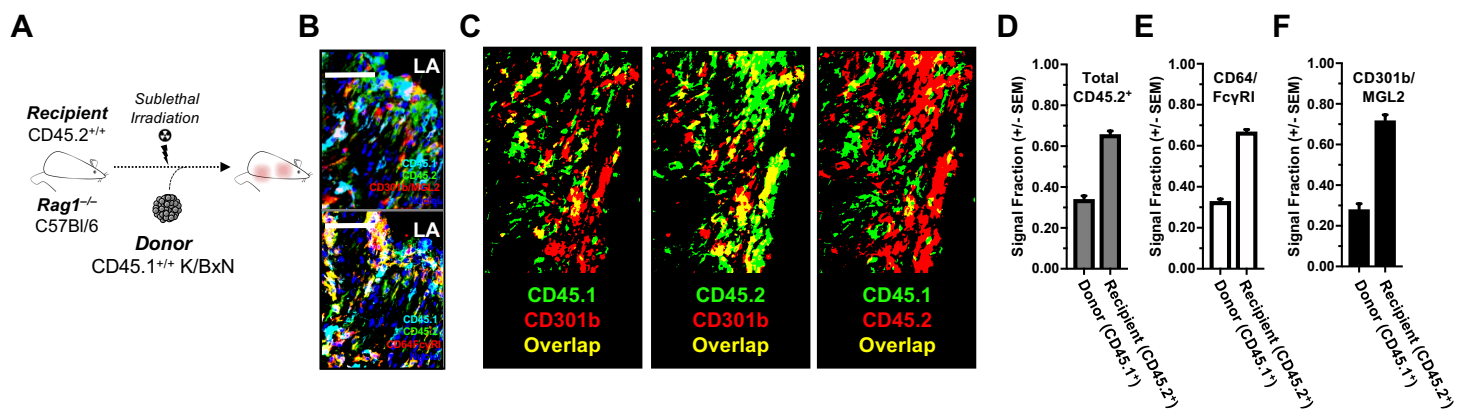
FIJI (ImageJ, NIH) was used for co-expression analyses. The auto-threshold function was used to convert grayscale images to binary. The threshold images were pseudo-colored either red (CD301b/MGL2, CD64/Fc γ RI) or green (CD45.1, CD45.2). After merging the respective red and green channels of interest (e.g. CD45.1 and CD301b/MGL2), co-expression was quantified as the number of yellow pixels (representing red and green co-localization) in each field of view.

The proportion of yellow pixels attributed to either CD45.1 or CD45.2 is shown. To quantify the relative abundance of leukocytes expressing either CD45.1 (bone marrow-derived) or CD45.2 (radio-resistant cell-derived), the total number of fluorescing pixels for each respective channel were summed and converted to a percentage of the total fluorescence originating from both the CD45.1 and the CD45.2 channels.

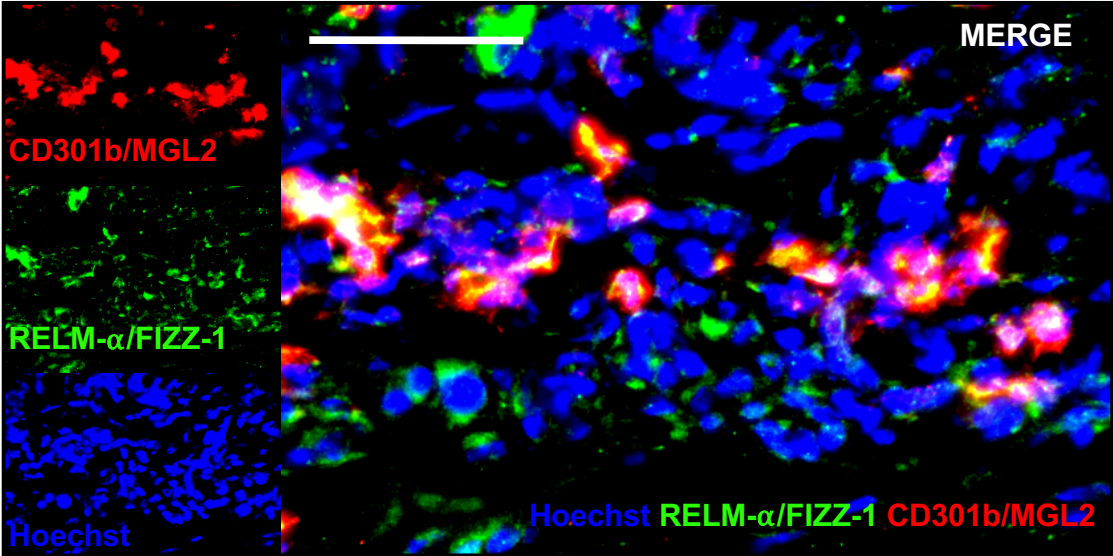
Anti-GPI titers and arthritis scoring

Determination of anti-GPI titers and clinical scoring of arthritis were conducted as described previously^{2, 3}.

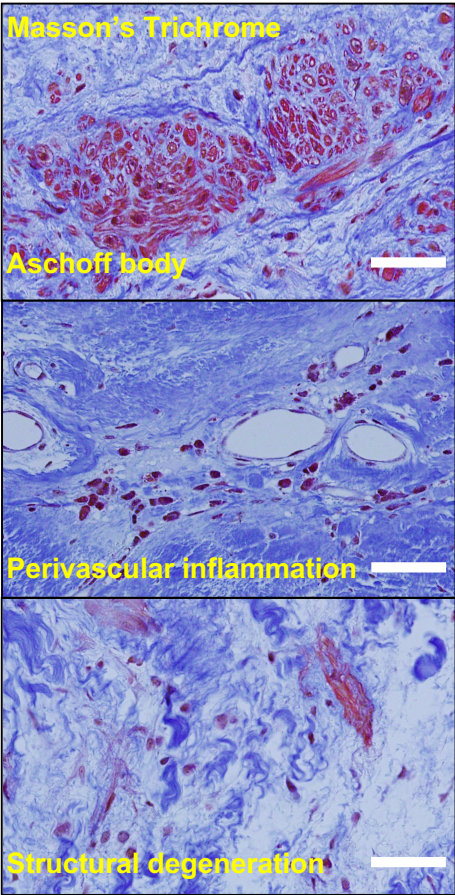
Supplemental Figure 1



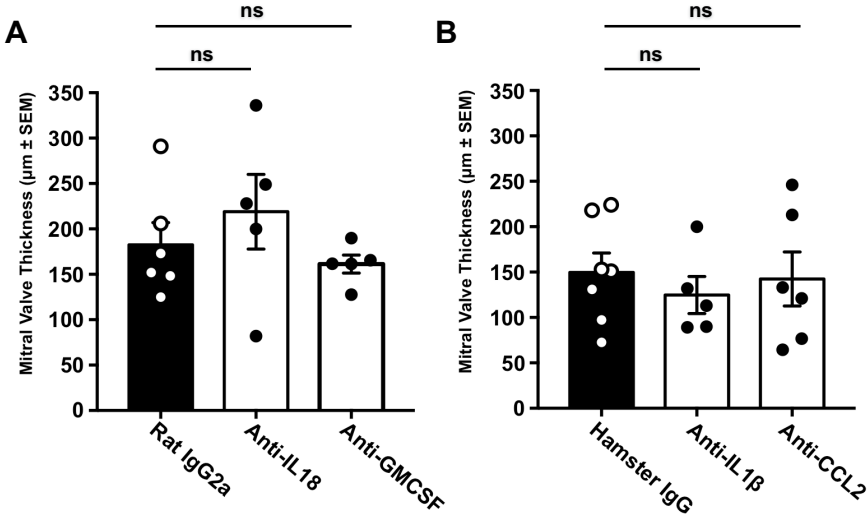
Supplemental Figure 2



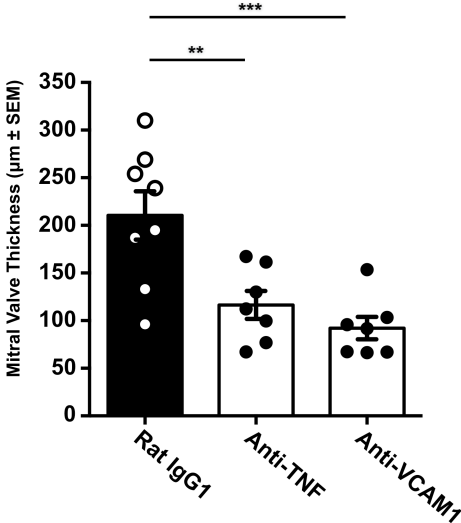
Supplemental Figure 3



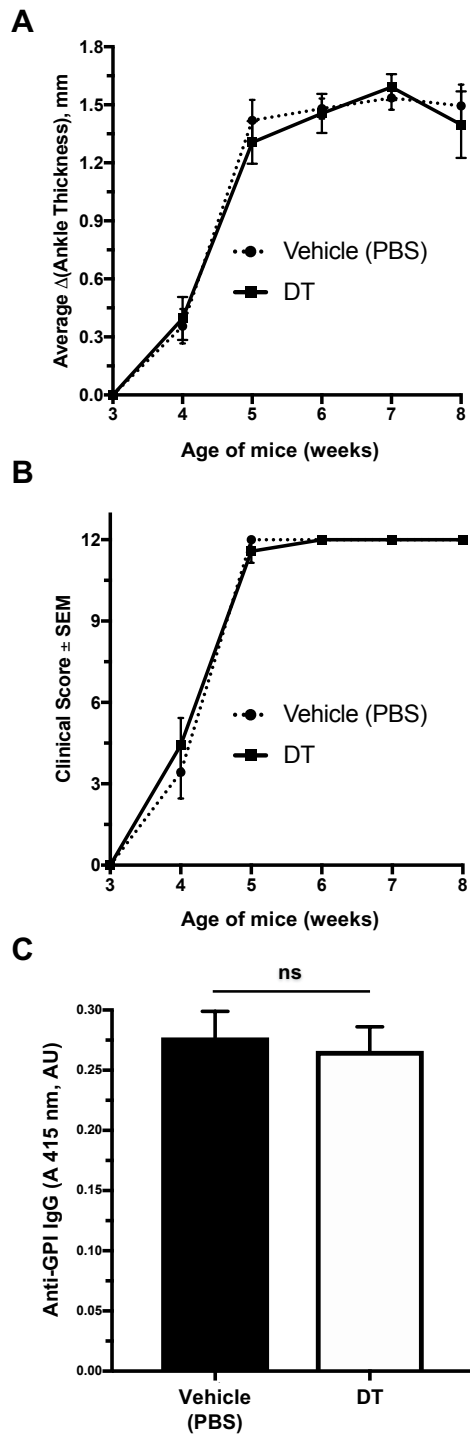
Supplemental Figure 4



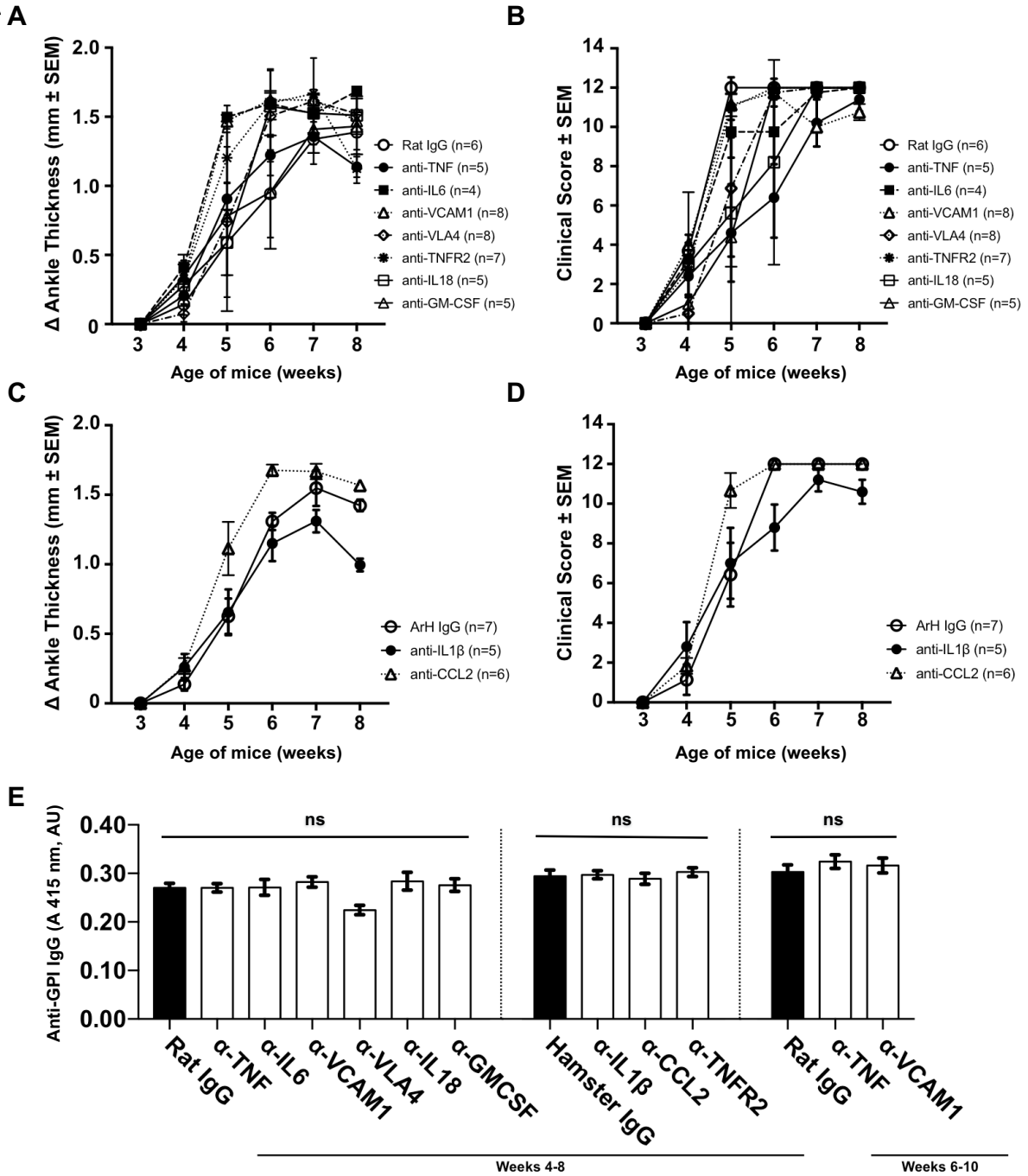
Supplemental Figure 5



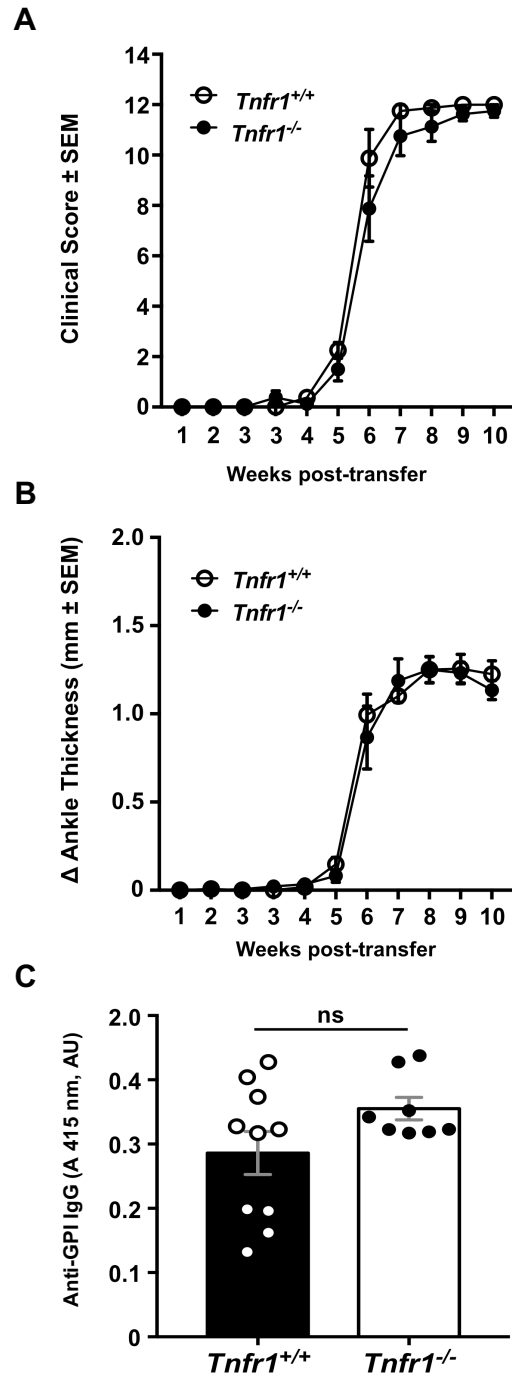
Supplemental Figure 6



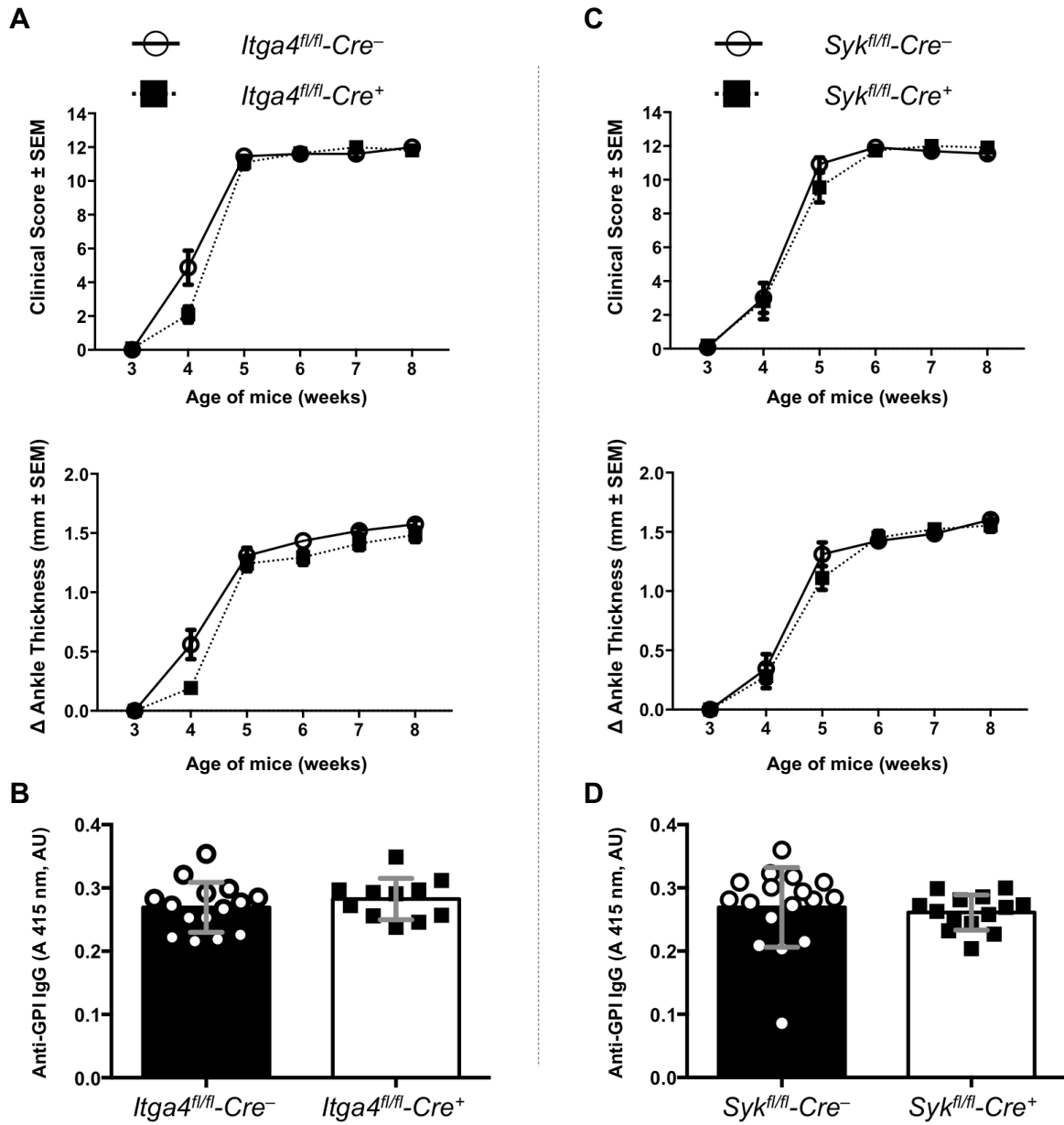
Supplemental Figure 7



Supplemental Figure 8



Supplemental Figure 9



SUPPLEMENTAL FIGURE LEGENDS

Supplemental Figure 1: Valve-infiltrating leukocytes primarily arise from radio-resistant populations while hematopoiesis provides a minor contribution to the inflammatory cell presence in K/B.g7 cardiac valves.

A, Experimental diagram for generation of CD45.1/CD45.2 bone marrow chimeric mice; CD45.2-expressing mice on the C57Bl/6 *Rag1*^{-/-} background were sub-lethally irradiated and reconstituted with 10⁷ cells from CD45.1-expressing K/B.g7 bone marrow. **B**, Representative combined, pseudo-colored MV IF images that were used in co-localization analysis. **C**, Applying a threshold to each of two channels of interest followed by pseudo-coloring either red or green (and vice versa for the second channel) allows quantification of pixels where both channels overlap (left: CD45.1: green, CD301b/MGL2: red, overlap: yellow; middle: CD45.2: green, CD301b/MGL2: red, overlap: yellow; left: CD45.1: green, CD45.2: red, overlap: yellow). **D**, Quantification of relative donor (CD45.1⁺) and recipient (CD45.2⁺) inflammatory cell presence in inflamed MVs (n=6). **E**, Quantification of the relative contribution to CD64/FcγRI-expressing cells arising from either CD45.1- or CD45.2-expressing cells (n=4). **F**, Quantification of the relative contribution of donor (CD45.1⁺) and host (CD45.2⁺) inflammatory cells to the CD301b/MGL2-expressing population (n=4). Scale bars are equal to 50 μm.

Supplemental Figure 2: A subset of MV-infiltrating CD301b/MGL2⁺ cells expresses resistin-like molecule-α (RELMα/FIZZ-1), a secreted protein associated with type-2 inflammation and fibrosis.

Immunofluorescence staining of K/B.g7 MVs for the type-2 inflammation and fibrosis-associated molecule, resistin like-molecule alpha (RELMα, a.k.a. found-in-inflammatory-zone-1 [FIZZ-1]) and CD301b/MGL2 (Hoechst 33342 used to counterstain nuclei). The scale bar in the merged image is equal to 50 μm.

Supplemental Figure 3: Histological features of rheumatic heart disease in patient samples.

A mitral valve (MV) specimen taken from a young adult male with mitral regurgitation (MR) secondary to rheumatic heart disease (RHD) demonstrating the presence of characteristic histopathological features including the presence of granulomatous inflammation (“Aschoff bodies”, top), perivascular inflammation (middle), and structural degeneration (bottom).

Supplemental Figure 4. Neutralization of specific pro-inflammatory mediators does not affect MV inflammation and fibrosis in K/B.g7 mice.

A, MV thicknesses measured following monoclonal antibody (mAb) blockade of interleukin-18 and granulocyte-macrophage colony stimulating factor (GM-CSF) between weeks 4-8, relative to species-matched isotype control antibody treated animals (black bar, left). **B**, MV thickness measured histologically following mAb-blockade of interleukin-1 β and chemokine (C-C motif) ligand 2 (CCL2/monocyte chemoattractant protein-1 [MCP-1]), relative to species matched isotype control-treated animals. Sample sizes are shown. ‘ns’ indicates no statistically significant difference between groups. The lack of statistical differences in both cases was determined using one-way analysis of variance (ANOVA) with post-hoc Tukey’s test for multiple comparisons.

Supplemental Figure 5: TNF and VCAM-1 inhibition during established MV disease prevents progression.

Maximum MV thickness in K/B.g7 mice that began treatment after disease onset (between weeks 6-10, in contrast to the 4-8 week regimen employed previously) with neutralizing monoclonal antibodies to TNF (middle) and VCAM-1 (right) in comparison to isotype control (rat IgG1, left)-treated animals. Asterisks denote significant differences as follows: ** $p < 0.01$, *** $p < 0.005$. Sample sizes are as follows (left-to-right): $n = 8, 7, 7$. Statistical differences were

assigned using one-way analysis of variance (ANOVA) with post-hoc Tukey's test for multiple comparisons.

Supplemental Figure 6. Anti-GPI titers and arthritis progression in *Mgl2-DTR* experiments

A, Average arthritis scores in DT- and vehicle-treated *Mgl2-DTR* mice. **B**, Average change in ankle thickness during the experimental duration in both DT- and vehicle-treated animals. **C**, Anti-glucose-6-phosphate-isomerase (GPI) titers in serum from K/B.g7:*Mgl2-DTR* mice treated with either diphtheria toxin (DT) or vehicle (PBS) during weeks 4-8. Sample sizes are as follows: DT: n=7; vehicle: n=7. Error bars represent the standard error of the mean (SEM).

Supplemental Figure 7. Arthritis development and anti-GPI titers in monoclonal antibody neutralization studies.

A, Relative increase in ankle thickness from baseline throughout the experimental duration for monoclonal antibody (mAb) blockade studies using rat antibodies. **B**, Averaged arthritis clinical scores for all mAb blockade studies that employed rat antibodies. **C**, Relative increase in ankle thickness from baseline throughout the experimental duration for monoclonal antibody (mAb) blockade studies using Armenian hamster antibodies. **D**, Averaged arthritis clinical scores for all mAb blockade studies that employed Armenian hamster antibodies. **E**, ELISA quantification of anti-GPI titers in serum samples taken from animals treated with mAb blockade; the lack of statistical differences (indicated by 'ns') in all cases was determined using one-way of variance (ANOVA) with post-hoc Tukey's test for multiple comparisons.

Supplemental Figure 8. Arthritis development and anti-GPI titers for *Tnfr1*^{-/-} bone marrow chimera studies.

A, Averaged arthritis clinical scores for BM chimera recipients in TNFR1-knockout studies. **B**, Relative increase in ankle thickness from baseline throughout the experimental duration in

TNFR1 bone marrow chimeric mice. **C**, ELISA quantification of anti-GPI titers in serum samples taken from BM chimera recipient mice at the experimental endpoint. 'ns' denotes no statistical difference between groups. Sample sizes are shown.

Supplemental Figure 9. Kinetics of arthritis development in conditional knockout lines.

A, Compiled arthritis clinical scores (top panel) and changes in ankle thickness (middle panel) during the experimental course for *Itga4* conditional deletion studies. **B**, Measurement of anti-GPI titers in serum taken at the experimental endpoint for conditional *Itga4* deletion studies. **C**, Compiled arthritis clinical scores (top panel) and changes in ankle thickness (middle panel) during the experimental course of *Syk* conditional deletion studies. **D**, Measurement of anti-GPI titers in serum taken at the experimental endpoint for conditional *Syk* deletion studies.

SUPPLEMENTAL REFERENCES

1. Verma M, Murkonda BS, Asakura Y, Asakura A. Skeletal Muscle Tissue Clearing for LacZ and Fluorescent Reporters, and Immunofluorescence Staining. *Methods Mol Biol.* 2016;1460:129-140. doi:10.1007/978-1-4939-3810-0_10.
2. Lee DM, Friend DS, Gurish MF, Benoist C, Mathis D, Brenner MB. Mast cells: a cellular link between autoantibodies and inflammatory arthritis. *Science.* 2002;297:1689-1692. doi:10.1126/science.1073176.
3. Nguyen LT, Jacobs J, Mathis D, Benoist C. Where FoxP3-dependent regulatory T cells impinge on the development of inflammatory arthritis. *Arthritis Rheum.* 2007;56:509-520. doi:10.1002/art.22272.